Array comparative genomic hybridization in retinoma and retinoblastoma tissues

Katia Sampieri,[1] Mariangela Amenduni,[1] Filomena Tiziana Papa,[1] Eleni Katzaki,[1] Maria Antonietta Mencarelli,[1] Annabella Marozza,[1] Maria Carmela Epistolato,[2] Paolo Toti,[2] Stefano Lazzi,[2] Mirella Bruttini,[1] Roberta De Filippis,[1] Sonia De Francesco,[3] Ilaria Longo,[1] Ilaria Meloni,[1] Francesca Mari,[1] Antonio Acquaviva,[4] Theodora Hadjistilianou,[3] Alessandra Renieri[1,5] and Francesca Ariani[1]

[1]Medical Genetics, Department of Molecular Biology, University of Siena, Policlinico Le Scotte, viale Bracci 2, 53100 Siena, Italy, [2]Department of Human Pathology and Oncology, University of Siena, Policlinico Le Scotte, viale Bracci 2, 53100, Siena, Italy, [3]Retinoblastoma Referral Center, Department of Ophtalmology, University of Siena, Policlinico Le Scotte, viale Bracci 2, 53100, Siena, Italy, [4]Department of Pediatrics, Obstetrics and Reproductive Medicine, Italian retinoblastoma registry, University of Siena, Policlinico Le Scotte, viale Bracci 2, 53100, Siena, Italy

(Received September 4, 2008/Revised November 17, 2008/Accepted November 19, 2008/Online publication January 31, 2009)

In retinoblastoma, two *RB1* mutations are necessary for tumor development. Recurrent genomic rearrangements may represent subsequent events required for retinoblastoma progression. Array-comparative genomic hybridization was carried out in 18 eye samples, 10 from bilateral and eight from unilateral retinoblastoma patients. Two unilateral cases also showed areas of retinoma. The most frequent imbalance in retinoblastomas was 6p gain (40%), followed by gains at 1q12-q25.3, 2p24.3-p24.2, 9q22.2, and 9q33.1 and losses at 11q24.3, 13q13.2-q22.3, and 16q12.1-q21. Bilateral cases showed a lower number of imbalances than unilateral cases ($P = 0.002$). Unilateral cases were divided into low-level (≤4) and high-level (≥7) chromosomal instability groups. The first group presented with younger age at diagnosis (mean 511 days) compared with the second group (mean 1606 days). In one retinoma case ophthalmoscopically diagnosed as a benign lesion no rearrangements were detected, whereas the adjacent retinoblastoma displayed seven aberrations. The other retinoma case identified by retrospective histopathological examination shared three rearrangements with the adjacent retinoblastoma. Two other gene-free rearrangements were retinoma specific. One rearrangement, dup5p, was retinoblastoma specific and included the *SKP2* gene. Genomic profiling indicated that the first retinoma was a pretumoral lesion, whereas the other represents a subclone of cells bearing 'benign' rearrangements overwhelmed by another subclone presenting aberrations with higher 'oncogenic' potential. In summary, the present study shows that bilateral and unilateral retinoblastoma have different chromosomal instability that correlates with the age of tumor onset in unilateral cases. This is the first report of genomic profiling in retinoma tissue, shedding light on the different nature of lesions named 'retinoma'. (*Cancer Sci* 2009; 100: 465–471)

Retinoblastoma (RB, OMIM#180200) is the most common primary intraocular malignancy in children, initiated by the inactivation of both alleles of the *RB1* tumor-suppressor gene.[1,2] Approximately 40% of RB patients carry a predisposing germline mutation transmitted as an autosomal-dominant trait. In these patients, inactivation of the second *RB1* allele occurs in the retinal cells and generally results in multiple and often bilateral tumors. In the remaining 60% of children, both mutational events occur in the same retinal cell leading to unilateral sporadic RB.[3]

Retinoma (RN), a benign retinal lesion, is considered to be the precursor of RB.[4,5] Unlike RB, which is typically opaque white, RN appears as a translucent gray retinal mass, frequently associated with calcification and retinal pigment epithelial hyperplasia.[6] The histopathology of RN includes foci of photoreceptor differentiation (fleurettes), momomorphic round nuclei, abundant fibrillar eosinophilic stroma, and absence of mitotic activity.[7] Recently, it has been demonstrated that the two mutational events inactivating the *RB1* gene are already present in RN.[4] Using quantitative polymerase chain reaction (PCR) and fluorescence *in situ* hybridization on specific candidate genes, it has also been shown that RN display low-level copy number changes involving higher levels of amplification in adjacent RB.[4,5] A study by Dimaras *et al*. in RN importantly clarified that the two hits in *RB1* (M1–M2) do not inevitably cause a malignant phenotype but only genomic instability.[4] At some point this instability can lead to further genomic rearrangements (M3–Mn) that result in tumor progression.[4,8]

Cytogenetic and conventional or microarray comparative genomic hybridization (CGH) studies have detected recurrent genomic alterations in RB: gain of 1q, 2p, 6p, and 13q and loss of 16q.[9] These data strongly suggest that these changes may represent M3–Mn events driving tumor progression in RB. In this scenario, RN represents a very interesting tissue to study the timing of genomic instability in RB development. However, molecular studies in this lesion are limited by sample availability as patients with only RN are not treated, and the coexistence of RN and RB in enucleated eyes is not frequently observed.[4,5]

Array-based CGH technology, designed for detecting segmental genomic alterations at high resolution, have enabled the profiling of human cancer genomes, defining regions and genes involved in cancer development and progression.[10–12] To date, genomic rearrangements in RB tissues have been principally investigated by cytogenetic and conventional CGH and only one array-CGH study has been published.[13–18] To our knowledge, genome-wide studies in RN tissues have never been carried out.

Here, we used a high-resolution array-CGH technique to analyze genomic rearrangements in 18 RB eye samples, 10 from bilateral and eight from unilateral patients. In two unilateral cases, we also investigated genomic imbalances in two areas of RN adjacent to RB.[5] In one case (#16), clinically diagnosed RN was observed to progress to RB, whereas in the other case (#15) RN was identified by retrospective histopathological examination.[5]

Materials and Methods

Tissue sample collection. We collected 18 formalin-fixed paraffin-embedded eye samples from enucleated RB patients archived in the Department of Human Pathology and Oncology of the University of Siena. After surgery, enucleated eyes were immersion-fixed in buffered formalin for 48 h. After fixation, sampling, paraffin embedding, and cutting were carried out according to the usual pathological methods. The group of samples included 10 bilateral cases (one familial and nine sporadic) and eight sporadic unilateral cases. For each patient we have the corresponding DNA sample

[5]To whom correspondence should be addressed. E-mail: renieri@unisi.it

doi: 10.1111/j.1349-7006.2008.01070.x

extracted from blood stored in the Italian Retinoblastoma Biobank (http://www.biobank.unisi.it). Samples 1–18 of the present study correspond to RB Biobank samples 15, 58, 143, 185, 190, 225, 134, 133, 234, 263, 79, 268, 242, 296, 297, 206, 253, and 279. A germline mutation in *RB1* was identified in 8 of 10 patients with bilateral tumors. No mutations were detected in the eight unilateral cases. Mutational screening was carried out by a combination of both DHPLC and MLPA analysis. Two unilateral cases presented areas of RN adjacent to RB.[5]

Laser-capture microdissection and DNA extraction from tissue samples. Normal retina, RN, and RB tissues were identified in hematoxylin–eosin-stained sections. Sections 5 μm thick were deparaffinized, rehydrated, and stained with Mayer hematoxylin and yellow eosin, then dehydrated with xylene. Slides were observed through an inverse microscope. Cells of the three different tissues were isolated by laser-capture microdissection (Arcturus PixCell II; MWG-Biotech). Selected cells adhered to the film on the bottom of the cap and were immediately transferred into a standard microcentrifuge tube containing digestion buffer and 20 μg/mL proteinase K (Qiagen). DNA was extracted using QIAmp DNA Micro Kit according to the manufacturer's protocol. The Hoechst dye-binding assay was used on a DyNA Quant 200 Fluorometer (GE Healthcare) to determine the appropriate DNA concentration.

Whole-genome amplification. Whole-genome amplification was carried out using the GenomePlex Complete Whole Genome Amplification (WGA) kit (Sigma-Aldrich) according to the manufacturer's protocol. Briefly, after DNA extraction from microdissected tissue cells, 100 ng of template DNA was incubated at 95°C for 4 min in 1× fragmentation buffer, and the sample was cooled on ice. The sample was further incubated with the Library Preparation Buffer and Library Stabilization Solution at 95°C for 2 min and then cooled on ice. One microliter of Library Preparation Enzyme was added and the mix incubated at 16°C for 20 min, 24°C for 20 min, 37°C for 20 min, and 75°C for 5 min. The resulting sample was amplified using WGA polymerase, after initial denaturation at 95°C for 3 min, then 14 cycles at 94°C for 15 s and 65°C for 5 min. Amplification products were purified using the GenElute PCR Clean-up kit (Sigma-Aldrich) according to the instructions of the suppliers. The appropriate DNA concentration was determined using a DyNA Quant 200 Fluorometer. Amplified DNA fragments from normal retina, RN, and RB samples varied in length from 200 to 500 bp.

Array-CGH. Array-CGH analysis was carried out using commercially available oligonucleotide microarrays containing approximately 99 000 60-mer probes with an estimated average resolution of approximately 25 kb (Human Genome CGH Microarray 105 A Kit; Agilent Technologies). DNA labeling was carried out using the Agilent Genomic DNA Labeling Kit Plus according to the Agilent protocol (Oligonucleotide Array-Based CGH for Genomic DNA Analysis 2.0v). Genomic DNA (3.5 μg) was mixed with 5 μL of 2.5× random primer solution (Agilent Technologies) and nuclease-free water to a total volume of 31 μL. The mix was denaturated at 95°C for 3 min and then incubated in ice and water for 5 min. The following were added to each sample: 10 μL of 5× buffer, 5 μL of 10× dNTP nucleotide mix, 1 μL of Klenow fragment (Agilent Technologies), and 3 μL of Cy5-dNTP (RB and RN samples) or 3 μL of Cy3-dNTP (normal retina samples). The samples were incubated at 37°C for 3 h. Labeled samples were subsequently purified using a CyScribe GFX Purification Kit (Amersham Biosciences) according to the manufacturer's protocol. Test and control DNA was pooled and mixed with 25 μg Human CotI DNA (Invitrogen), 26 μL blocking buffer (Agilent Technologies), and 130 μL hybridization buffer (Agilent Technologies). Before hybridization to the array, the mix was denatured at 95°C for 5 min then pre-associated at 37°C for 1 h. Probes were applied to the slide using an Agilent microarray hybridization station. Hybridization was carried out for 40 h at 65°C in a rotating oven ($0.040 \times g$). The array was disassembled and washed with wash buffers supplied with the Agilent 105 A kit. The slides were dried and scanned using an Agilent G2565BA DNA microarray scanner.

Image and data analysis. Image analysis was carried out using CGH Analytics Software v. 3.4.40 (Agilent Technologies) with default settings. The software automatically determines the fluorescence intensities of the spots for both fluorochromes, performing background subtraction and data normalization, and compiles the data into a spreadsheet that links the fluorescent signal of every oligonucleotide on the array to the oligonucleotide name, its position on the array, and its position in the genome. The linear order of the oligonucleotides is reconstituted in the ratio plots consistent with an ideogram. The ratio plot is arbitrarily assigned such that gains and losses in DNA copy number at a particular locus are observed as a deviation of the ratio plot from a modal value of 1.0. DNA sequence information refers to the public University of California, Santa Cruz (UCSC) database (Human Genome Browser, http://genome.ucsc.edu, May 2004 assembly).

Real-time quantitative PCR analysis. Real-time quantitative PCR was carried out to confirm array-CGH data. For recurrent rearrangements, we used probes already reported in a previous manuscript by Sampieri *et al*. (2008) and new custom-made TaqMan probes (Applied Biosystems) designed for the *RB1* and *RBL2* genes (Supplementary Table 1). By using custom-made assays, we also confirmed the RN and RB (*SKP2*-specific probe) private imbalances found in case #15 (Table 4) (Supplementary Table 1). PCR reactions and data analysis were carried out as previously described.[5]

Statistical analysis. We used the Mann–Whitney *U*-test to compare means of continuous variables between the two groups. *P*-values ≤0.05 were considered significant.

Results

Array-CGH analysis in RB samples. Using array-CGH, we investigated genomic rearrangements in 18 eye tissues, 10 from bilateral and eight from unilateral RB patients. Array-CGH analysis identified genomic rearrangements in 12 of 18 tumor samples (~67%).

In total, we found 64 genomic aberrations, mostly gains (47 gains vs 17 losses) (Table 1). The number of rearrangements was significantly different (Mann–Whitney *U*-test, $P = 0.002$) between the two groups of patients: bilateral cases showed a lower number of imbalances (mean 1; range 0–4) compared with unilateral cases (mean 7; range 2–24) (Table 1).

Recurrent imbalances involved chromosomes 1, 2, 6, 9, 11, 13, and 16 (Fig. 1) (Table 2). In 7 of 18 (40%) samples the entire p arm of chromosome 6 was duplicated (Table 2). The other cases bearing overlapping rearrangements defined minimal common regions of gain (MRG) or loss (MRL): dup(1)(q12; q25.3) (4/18 samples; 22%), dup(2)(p24.3; p24.2) (4/18 samples; 22%), dup(9)(q22.2) (3/18 samples; 17%), dup(9)(q33.1) (2/18 samples; 11%), del(11)(q24.3) (2/18 samples; 11%), del(13)(q13.2-q22.3) (2/18 samples; 11%), and del(16)(q12.1-q21) (2/18 samples; 11%) (Fig. 1) (Table 2). Recurrent regions of gain or loss have been confirmed by real-time quantitative PCR (Supplementary Table 1).

These regions have been studied for gene content to identify candidates involved in RB progression. We first searched for known oncogenes and tumor suppressors (Table 2). Based on annotated gene function, we selected additional candidates (Table 2). Priority was given to genes participating in the pRB pathway and to genes playing a role in the mechanisms of cell proliferation, differentiation, apoptosis, or senescence (Table 2).

Correlating molecular and clinical data, we found that in unilateral cases the number of rearrangements is associated with age at diagnosis (Table 3). The group with low-level chromosomal instability (≤4 chromosomal aberrations) presented with a younger age at diagnosis (mean 511 days; range 90–958 days), whereas the group with high-level chromosomal instability (≥7 chromosomal aberrations) were older at diagnosis (mean 1606 days; range 1326–1828 days) (Table 3).

doi: 10.1111/j.1349-7006.2008.01070.x

Table 1. Chromosomal aberrations detected by array-comparative genomic hybridization in 18 retinoblastomas

Case no.	Phenotype	No. aberrations	aCGH gains	aCGH losses
1	B	0	/	/
2	B	0	/	/
3	B	0	/	/
4	B	0	/	/
5	B	0	/	/
6	B	0	/	/
7	B	1	2 p24.3-p24.2{2.15 Mb}	
8	B	2	6p25.3-p11.1{58.7 Mb}	5q34{13.83 Mb}
9	B	2	2p24.3{3.75 Mb} 6p25.3-p11.1{58.7 Mb}	
10	B	4		2q32.1{0.43 Mb} 4q28.3{0.40 Mb} 7q31.1{0.70 Mb} 8q21.3{0.35 Mb}
11	U	2	6p25.3-p11.1{58.7 Mb}	13q12.11–13q31.2{69.77 Mb}
12	U	2	2p25.3-p22.3{34.85 Mb} 6p25.3-p11.1{58.7 Mb}	
13	U	4	1q12-q25.3{38.17 Mb} 3q26.1-q29{32.80 Mb} 9q12-q34.3{50.30 Mb}	13q13.2-q22.3{44.90 Mb}
14	U	4	1p35.3-q44{217.70 Mb} 6p25.3-p11.1{58.7 Mb} 7q34-q36.3{21.30 Mb}	9p24.3-p23{12.59 Mb}
15	U	4	5p15.33-p12{46.14 Mb} 5q13.2{0.70 Mb} 6p25.3-p11.1{58.7 Mb} 8p23.1{0.60 Mb}	
16	U	7	1q21.1-q44{104.50 Mb} 2p25.3-p22.3{35.55 Mb}	1p32.1-p12{58.4 Mb} 4p16.3-p14{37.6 Mb} 11q22.3-q25{28.0 Mb} 12p13.33-p13.1{14.2 Mb} 16q12.1-q21{7.1 Mb}
17	U	8	1q12-q44{104.50 Mb} 6p25.3-p11.1{58.7 Mb} 9q22.2{0.23 Mb} 20q13.33{0.24 Mb}	7p13{0.66 Mb} 14q11.2-q21.1{23.25 Mb} 15q23{0.30 Mb} 16q11.2-q24.3{43.66 Mb}
18	U	24	5q33.1{0.35 Mb} 7p15.2{0.23 Mb} 8q24.23{0.28 Mb} 9q22.2{0.58 Mb} 9q33.1{0.31 Mb} 10q23.1{0.15 Mb} 11q23.3{0.63 Mb} 12q24.32{0.16 Mb} 13q12.12{0.22 Mb} 13q13.3{0.31 Mb} 14q22.3{0.49 Mb} 17q25.3{0.28 Mb} 18q21.1{1.98 Mb} 18q22.3-q23{1.59 Mb} 20q13.12{0.20 Mb}	1p21.3{0.30 Mb} 2q11.2{0.28 Mb} 2q31.33{0.13 Mb} 2q37.3{0.13 Mb} 3q25.1{0.31 Mb} 4q26{0.39 Mb} 10p12.33{0.11 Mb} 11q24.3{0.58 Mb} 20p11.21{0.43 Mb}

B, bilateral cases; U, unilateral cases. The size of rearrangement is given in curly brackets.

Array-CGH analysis in RN samples. Two cases affected by unilateral RB (#15 and #16) showed areas of RN adjacent to the tumor. The RN of case #16 was clinically diagnosed as a benign lesion that underwent malignant transformation after 11 months, whereas the RN of case #15 was identified by retrospective histopathological examination. Detailed clinical and histopathological data of the two lesions have already been described in Sampieri *et al*.[5]

Array-CGH analysis did not detect any genomic rearrangement in the RN of patient #16. In contrast, five genomic rearrangements were identified in the RN of case #15 (Table 4). Among them, three were also in the adjacent RB (dup5q13.2, dup6p, dup8p23.1), whereas the remaining two (dup1q32.2 and dup13q31.2) were detected exclusively in the RN (Table 4). For the common rearrangement on 6p, array-CGH log ratio values indicated that the level of gain was progressively increased from RN (log ratio ~0.5) to RB (log ratio ~1.0) (Table 4). One rearrangement, dup5p, was present only in the RB (Table 4). RN- and RB-specific rearrangements have been confirmed by real-time quantitative PCR.

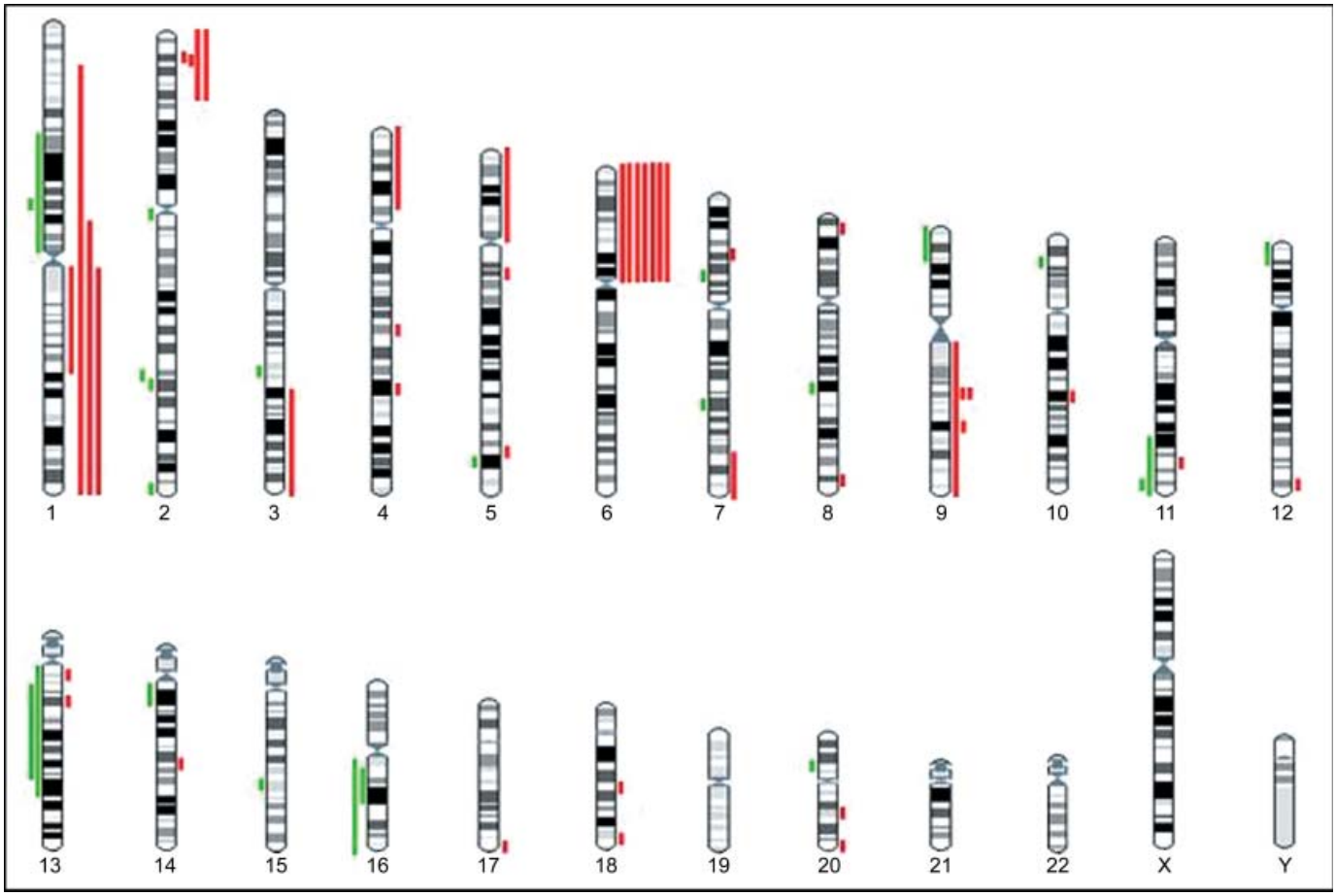

Fig. 1. Overview of rearranged chromosomal regions in 18 retinoblastomas as detected by array-comparative genomic hybridization. Lines on the left of each chromosome represent losses and lines on the right represent gains.

Table 2. Recurrent genomic imbalances identified by array-comparative genomic hybridization analysis

Chromosomal imbalances	Breakpoints	Frequency (%)	No. genes	Oncogenes and tumor suppressors	Other candidate genes
Dup(6)(p25.3; p11.1){58.7 Mb}	108 083 58 827 841	40 (7/18)	461	*IRF4*, *DEK*, *PIM1*	*E2F3*, *CCND3*
Dup(1)(q12; q25.3){38.17 Mb}†	141 465 960 179 620 513	22 (4/18)	497	/	*MCL1*, *SHC1*, *MUC1*
Dup(2)(p24.3; p24.2){2.15 Mb}†	15 120 360 17 242 742	22 (4/18)	4	*MYCN*	*DDX1*
Dup(9)(q22.2){0.23 Mb}†	90 484 233 90 687 380	17 (3/18)	2	/	/
Dup(9)(q33.1){0.31 Mb}	116 974 701 117 251 019	11 (2/18)	1	/	/
Del(11)(q24.3){0.58 Mb}†	127 676 090 128 202 918	11 (2/18)	2	/	*ETS1*
Del(13)(q13.2; q22.3){44.90 Mb}†	33 623 259 78 516 556	11 (2/18)	123	*RB1*, *ARLTS1*	/
Del(16)(q12.1; q21){7.02 Mb}†	50 674 625 57 636 204	11 (2/18)	67	/	*CYLD*, *RBL2*

†Minimal overlapping regions.

These regions have been studied for gene content in order to identify candidates involved in the RN–RB transition. We searched for known oncogenes and tumor suppressors, for genes related to the pRB pathway, and for genes involved in proliferation, differentiation, apoptosis, or senescence (Table 4).

Discussion

The loss of *RB1* function, by means of two mutational events (M1 and M2), is considered to be the first rate-limiting step in RB development.[1,4] Several studies have suggested that genomic

doi: 10.1111/j.1349-7006.2008.01070.x

Table 3. Correlation between the number of genomic rearrangements and age at diagnosis in unilateral cases

Case no.	No. rearrangements	Chromosomal instability group	Age at diagnosis (days)
11	2	≤4	90
12	2	≤4	743
13	4	≤4	285
14	4	≤4	480
15	4	≤4	958
16	7	≥7	1326
17	8	≥7	1663
18	24	≥7	1828

imbalances (M3–Mn) involving specific oncogenes and tumor suppressors are required for malignant transformation of RB.[9] In order to characterize such genomic changes, we used high-resolution array-CGH to investigate a series of 18 tumor samples (10 bilateral and eight unilateral) and two RN samples from enucleated RB patients.[5] To our knowledge this is the first genome-wide study in RN tissue.

In RB samples, we detected a total of 64 rearrangements: 47 gains and 17 losses (Table 1). Interestingly, bilateral cases showed a lower number of imbalances (mean 1) compared to unilateral cases (mean 7), with statistical significance ($P = 0.002$) (Table 1). We compared our data with results obtained in the only other array-CGH study carried out previously on RB tissues.[18] We found that, even if the resolution level was quite different (25 vs 500 kb), the results were in agreement and the number of rearrangements in unilateral cases was significantly higher than in bilateral cases.[18] These results suggest that, beyond the inactivation of both *RB1* alleles, different molecular mechanisms may be involved in tumor progression of hereditary RB. Apart from chromosomal instability, other genetic alterations can drive cancer progression, including subtle DNA sequence changes such as microsatellite instability, chromosomal translocations, and single-gene amplifications or deletions. All of these changes have been described in RB but systematic correlations with clinical data have never been carried out.[5,19–22]

In accordance with previous data, we found recurrent imbalances on chromosomes 1, 2, 6, 13, and 16 (Table 2).[9] Three previously undescribed recurrent rearrangements were identified, two on chromosome 9 and one on chromosome 11 (Table 2).

Gains of 6p showed the highest frequency (40%), confirming that it represents the most common change observed in RB.[9] The rearrangement contains 461 genes, including the three known oncogenes *IRF4*, *DEK*, and *PIM1* (Table 2). We further selected two members of the pRB pathway that have an essential role in G1–S cell-cycle transition: the pRB-regulated transcription factor E2F3 and cyclin CCND3, involved in pRB phosphorylation (Table 2).[23,24] Previous studies reporting more focused gains at 6p22 led to deep investigation of the genes within this region.[14] By QM-PCR and microarray expression analysis on RB tissues, it has been demonstrated that *DEK* and *E2F3* are the most commonly gained genes and that they show overexpression.[25,26] Furthermore, *DEK* and *E2F3* are overexpressed in Tag-RB murine tumors.[9] These results indicate that both *DEK* and *E2F3* represent strong candidates for RB progression and that a combination of genes on 6p, instead of a single one, probably contributes to RB progression.

The MRG on chromosome 1 (dup1q12-q25.3) contains 497 genes (Table 2). We selected *MUC1* as its overexpression, as found in human carcinomas and certain hematological malignancies, induces transformation and resistance to apoptosis (Table 2).[27,28] Other interesting candidates are *MCL1*, encoding a potent multi-domain antiapoptotic protein of the BCL2 family, and *SHC1*, a key intracellular signaling molecule that participates in the transforming activity of oncogenic tyrosine kinases (Table 2).[29,30] By array-CGH, Zielinski *et al*. also found recurrent 1q imbalances narrowing one MRG at 1q22 and indicated *SHC1* as a candidate.[18] Two previously identified strong candidates on 1q, *KIF14* and *MDM4*, were not included within the identified MRG. Using a gene-specific quantitative PCR approach, both genes have been found to be gained in RB.[5] In addition, their overexpression is well documented in RB tissues.[31,32] *KIF14* and *MDM4* may therefore play an important role in RB progression, regardless of 1q status.

The MRG defined on chromosome 2 contains only four genes, including the known oncogenes *MYCN* and *DDX1*, a gene that encodes a DEAD box protein probably involved in pre-mRNA 3′-end processing that has been shown to possess oncogenic properties (Table 2).[33] Importantly, *MYCN* and *DDX1* have been found to be coamplified and overexpressed in RB and neuroblastoma cell lines and tumors.[34]

The two small MRG detected on chromosome 9, dup(9)(q22.2) and dup(9)(q33.1), contain two genes and one gene, respectively (Table 2). None are reported as oncogenes or tumor suppressors and no obvious candidates have emerged.

Only two genes lie in the MRL defined on chromosome 11 (Table 2). The transcription factor ETS1 is involved in control of cellular proliferation, cell senescence and death, and tumorigenesis.[35] Its expression is correlated with more malignant carcinomas and is a negative prognostic indicator.[36]

Table 4. Genomic rearrangements identified in the retinoma (RN) and retinoblastoma (RB) of case #15

Chromosomal imbalances	Breakpoints	RN	RB	No. genes	Oncogenes and tumor suppressors	Other candidate genes
Dup(1)(q32.2){0.28 Mb}	205 507 621 205 754 022	+	–	0	/	/
Dup(5)(p15.33; p12){46.14 Mb}	110 640 46 008 694	–	+	121	/	*SKP2*
Dup(5)(q13.2){0.70 Mb}	69 741 318 70 422 297	+	+	7	/	*BIRC1*
Dup(6)(p25.3; 11.1){58.7 Mb}	126 650 58 721 961	+†	+†	461	*IRF4*, *DEK*, *PIM1*	*E2F3*, *CCND3*
Dup(8)(p23.1){0.60 Mb}	7 261 418 7 789 937	+	+	7	/	/
Dup(13)(q31.2){0.38 Mb}	87 587 852 87 622 748	+	–	0	/	/

Position of oligonucletides and genes refers to the UCSC (University of California, Santa Cruz) Genome Browser (http://genome.ucsc.edu, on Human, May 2004 assembly). †Log ratio values: ~0,5 in RN; ~1,0 in RB.

The MRL on chromosome 13 contains 123 genes (Table 2). Apart from *RB1*, this region bears the newly characterized tumor-suppressor gene *ARLTS1*.[37] It encodes a pro-apoptotic protein of the Ras superfamily involved in the pathogenesis of various types of tumors: two SNP have been found to influence familial cancer risk for B-CLL and *BRCA1*- and *BRCA2*-negative breast cancers, whereas DNA hypermethylation and genomic deletions have been identified as mechanisms of *ARLTS1* downregulation in CLL, lung cancers, and ovarian tumors.[38–41]

The MRL on chromosome 16 contains the *RBL2* gene, encoding RB family member p130 (Table 2). *RBL2* loss has been confirmed by real-time quantitative PCR. *RBL2* expression is reduced in RB tissues and is one of the genes that can be ablated along with *Rb1* to cause retinal tumor formation in mice.[42–44] This region also includes the familial cylindromatosis tumor-suppressor gene *CYLD*, whose loss inhibits the apoptotic pathway by activating nuclear factor-κB (Table 2).[45]

Correlating array-CGH results with age at diagnosis, we observed that, among unilateral cases, a higher number of chromosomal aberrations is associated with an older age (Table 3). These results are in accordance with a previous CGH study reporting that unilateral RB from children with an older age showed significantly more genetic abnormalities than RB from children with a younger age.[15] This could be due to the fact that a high level of genomic instability may lead to suppression of tumor growth, resulting in delayed disease onset.[46] It is also possible that an intrinsically slow growth rate of the tumor allows the accumulation of a higher number of chromosomal aberrations.

Sample #18, with the oldest age at diagnosis, had the highest number of genomic aberrations (24), all of which were small in size (0.11–1.98 Mb) (Tables 1,3). Interestingly, dup18q21.1 contains Sma- and Mad-related protein 2 (*SMAD2*), encoding a protein with sequence similarity to the *Mad2* gene product in *Drosophila*, a key component of the spindle checkpoint.[47,48] It has been demonstrated that hyperactivation of Mad2 by E2F1 leads to chromosomal instability and aneuploidy in cells in which the Rb pathway is disrupted.[49]

Array-CGH analysis of the RN tissues revealed strikingly different results in the two cases. RN from sample #16 did not present with any rearrangements, whereas seven alterations were detected in the adjacent RB (Table 1). Interestingly, one of the rearrangements (del16q12.1-q21) contains the *RBL2* gene. In a recent paper, Dimaras *et al*. found that p130 is highly expressed in RN but not in RB, suggesting that it represents a key factor differentiating the two lesions.[4] The authors also hypothesized that RB can emerge from stable RN by failure of senescence and that p130 may represent the effector of such a mechanism.[4,50]

In case #15, the RN showed five genomic rearrangements compared to normal retina, three of which were common to RB (Table 4). Concerning the common imbalance on 6p, the level of gain was higher in RB than RN, reinforcing the importance of candidate genes such as *DEK* and *E2F3* in malignant progression. The imbalance found in both tissues on 5q includes *BIRC1*, an interesting candidate gene for early retina–RN transition as it encodes a protein known to act as an inhibitor of apoptosis, directly suppressing caspases (Table 4).[51] Two rearrangements were found exclusively in RN and they do not contain any known genes (Table 4). Chromosomal gain on 5p, present only in RB, includes SKP2 (p45), an oncogenic protein found to be overexpressed in cancer (Table 4).[52] It displays an S-phase-promoting function and is implicated in the ubiquitin-mediated proteolysis of the Cdk inhibitor p27.[53–55] It has been demonstrated that cell-cycle arrest through the inhibition of cdk2 activity by p27 is critical for pRB-induced senescence.[56] Bypass of senescence could be therefore involved in malignant transformation of RB through the pRB–SKP2–p27 pathway.

The different genomic profiles obtained in the two lesions identified as RN, sharing the same histopathological appearance, indicate that they do indeed represent different entities. Case #16, which was clinically diagnosed as RN and was observed to progress to RB after 11 months, was a pretumoral lesion that had not yet acquired chromosomal aberrations. In a previous study, we showed by real-time quantitative PCR that RN displays gene-specific low-level gains, with higher levels in adjacent RB.[5] These results suggest that increased genomic instability, including chromosomal aberrations and progressive gene amplification, accompanies the RN–RB transition.

In contrast, the other case of RN (case #15), without clinically detectable RN that was identified by retrospective histopathological examination, represents a further step in RB progression. It appears as a subclone of cells bearing 'benign' rearrangements that has been overwhelmed by another subclone presenting aberrations with selective growth advantage, leading to outgrowth of the tumor. These data underline that only specific sets of chromosomal rearrangements can lead a tumor-cell precursor to overcome the selection barrier and generate a fully malignant phenotype.

In conclusion, array-CGH analysis carried out on 18 RB revealed a different chromosomal instability level between bilateral and unilateral cases. Among the unilateral group, a bimodal distribution of chromosomal changes was observed, which correlated with age of diagnosis. Already characterized recurrent genomic aberrations have been confirmed and three new ones have been detected, indicating candidate genes for RB progression. Finally, the present study represents the first report of genomic profiling in RN tissues and provides the basis for investigation of the role of chromosomal instability in the RN–RB transition.

Acknowledgments

This work was supported by a FIRB grant (RBIP00PMF2) to A.R., University of Siena grant PAR2006 to M.B., and a grant on retinoblastoma from Istituto Toscano Tumori to A.R.

Abbreviations

ARLTS1	ADP-Ribosylation factor-Like Tumor Suppressor 1
BCL2	B-cell CLL/Lymphoma 2
B-CLL	B-Cell Chronic Lymphocytic Leukemia
BIRC1	Baculoviral IAP Repeat-Containing protein 1
BRCA	Breast Cancer
CCND3	Cyclin D3
Cdk	Cyclin-dependent kinases
CLL	Chronic Lymphocytic Leukemia
CYLD	Cylindromatosis
DDX1	DEAD (Asp-Glu-Ala-Asp) Box polypeptide 1
DEK	DEK oncogene
DHPLC	Denaturing High Performance Liquid Chromatography
E2F3	E2F transcription factor 3
ETS1	V-ETS erythroblastosis virus E26 oncogene homolog 1 (avian)
FIRB	Fondo Investimenti Ricerca di Base
IRF4	Interferon Regulatory Factor 4
KIF14	Kinesin Family member 14
MCL1	Myeloid Cell Leukemia 1
MDM4	Mouse Double Minute 4 homolog
MLPA	Multiplex Ligation-dependent Probe Amplification
MUC1	MUCIN 1
MYCN	V-MYC avian myelocytomatosis viral-related oncogene, Neuroblastoma-derived
PIM1	PIM 1 oncogene
pRB	Retinoblastoma protein
QM	Quantitative Multiplex
RB1	Retinoblastoma
RBL	retinoblastoma-like
RBL2	retinoblastoma-like 2
SHC1	Src (homology 2 domain containing) transforming protein
SKP2	S-phase Kinase-associated Protein 2
SNP	Single Nucleotide Polymorphism
WGA	Whole Genome Amplification

doi: 10.1111/j.1349-7006.2008.01070.x

References

1 Knudson AG Jr. Mutation and cancer: statistical study of retinoblastoma. *Proc Natl Acad Sci USA* 1971; **68**: 820–3.
2 Abramson DH, Schefler AC. Update on retinoblastoma. *Retina* 2004; **24**: 828–48.
3 Vogel F. Genetics of retinoblastoma. *Hum Genet* 1979; **52**: 1–54.
4 Dimaras H, Khetan V, Halliday W *et al*. Loss of RB1 induces non-proliferative retinoma: increasing genomic instability correlates with progression to retinoblastoma. *Hum Mol Genet* 2008; **17**: 1363–72.
5 Sampieri K, Mencarelli MA, Epistolato MC *et al*. Genomic differences between retinoma and retinoblastoma. *Acta Oncol* 2008; **47**: 1483–92.
6 Gallie BL, Ellsworth RM, Abramson DH, Phillips RA. Retinoma: spontaneous regression of retinoblastoma or benign manifestation of the mutation? *Br J Cancer* 1982; **45**: 513–21.
7 Margo C, Hidayat A, Kopelman J, Zimmerman LE. Retinocytoma: A benign variant of retinoblastoma. *Arch Ophthalmol* 1983; **101**: 1519–31.
8 Gallie BL, Campbell C, Devlin H, Duckett A, Squire JA. Developmental basis of retinal-specific induction of cancer by RB mutation. *Cancer Res* 1999; **59**: 1731s–5s.
9 Corson TW, Gallie BL. One hit, two hits, three hits, more? Genomic changes in the development of retinoblastoma. *Genes Chromosomes Cancer* 2007; **46**: 617–34.
10 Solinas-Toldo S, Lampel S, Stilgenbauer S *et al*. Matrix-based comparative genomic hybridization: biochips to screen for genomic imbalances. *Genes Chromosomes Cancer* 1997; **20**: 399–407.
11 Pinkel D, Segraves R, Sudar D *et al*. High resolution analysis of DNA copy number variation using comparative genomic hybridization to microarrays. *Nat Genet* 1998; **20**: 207–11.
12 Davies JJ, Wilson IM, Lam WL. Array CGH technologies and their applications to cancer genomes. *Chromosome Res* 2005; **13**: 237–48.
13 Mairal A, Pinglier E, Gilbert E *et al*. Detection of chromosome imbalances in retinoblastoma by parallel karyotype and CGH analyses. *Genes Chromosomes Cancer* 2000; **28**: 370–9.
14 Chen D, Gallie BL, Squire JA. Minimal regions of chromosomal imbalance in retinoblastoma detected by comparative genomic hybridization. *Cancer Genet Cytogenet* 2001; **129**: 57–63.
15 Herzog S, Lohmann DR, Buiting K *et al*. Marked differences in unilateral isolated retinoblastomas from young and older children studied by comparative genomic hybridization. *Hum Genet* 2001; **108**: 98–104.
16 Lillington DM, Kingston JE, Coen PG *et al*. Comparative genomic hybridization of 49 primary retinoblastoma tumors identifies chromosomal regions associated with histopathology, progression, and patient outcome. *Genes Chromosomes Cancer* 2003; **36**: 121–8.
17 van der Wal JE, Hermsen MA, Gille HJ *et al*. Comparative genomic hybridisation divides retinoblastomas into a high and a low level chromosomal instability group. *J Clin Pathol* 2003; **56**: 26–30.
18 Zielinski B, Gratias S, Toedt G *et al*. Detection of chromosomal imbalances in retinoblastoma by matrix-based comparative genomic hybridization. *Genes Chromosomes Cancer* 2005; **43**: 294–301.
19 Choy KW, Pang CP, Fan DS *et al*. Microsatellite instability and MLH1 promoter methylation in human retinoblastoma. *Invest Ophthalmol Vis Sci* 2004; **45**: 3404–9.
20 Dries D, Baca K, Truss L, Dobin S. Interstitial deletion of 13q and a 13; X chromosome translocation results in partial trisomy 13 and bilateral retinoblastoma. *Ophthalmic Genet* 2003; **24**: 175–80.
21 Howard RO. Multiple changes in oncogenes and tumor suppressor genes in human retinoblastoma. *Trans Am Ophthalmol Soc* 1996; **94**: 299–312.
22 Bowles E, Corson TW, Bayani J *et al*. Profiling genomic copy number changes in retinoblastoma beyond loss of RB1. *Genes Chromosomes Cancer* 2007; **46**: 118–29.
23 Wu L, Timmers C, Maiti B *et al*. The E2F1-3 transcription factors are essential for cellular proliferation. *Nature* 2001; **414**: 457–62.
24 Shu F, Lv S, Qin Y *et al*. Functional characterization of human PFTK1 as a cyclin-dependent kinase. *Proc Natl Acad Sci USA* 2007; **104**: 9248–53.
25 Grasemann C, Gratias S, Stephan H *et al*. Gains and overexpression identify DEK and E2F3 as targets of chromosome 6p gains in retinoblastoma. *Oncogene* 2005; **24**: 6441–9.
26 Orlic M, Spencer CE, Wang L, Gallie BL. Expression analysis of 6p22 genomic gain in retinoblastoma. *Genes Chromosomes Cancer* 2006; **45**: 72–82.
27 Agata N, Ahmad R, Kawano T, Raina D, Kharbanda S., Kufe D. MUC 1 oncoprotein blocks death receptor-mediated apoptosis by inhibiting recruitment of caspase-8. *Cancer Res* 2008; **68**: 6136–44.
28 Raina D, Ahmad R, Kumar S *et al*. MUC1 oncoprotein blocks nuclear targeting of c-Abl in the apoptotic response to DNA damage. *EMBO J* 2006; **25**: 3774–83.
29 Mott JL, Kobayashi S, Bronk SF, Gores GJ. mir-29 regulates Mcl-1 protein expression and apoptosis. *Oncogene* 2007; **26**: 6133–40.
30 McGlade J, Cheng A, Pelicci G, Pelicci PG, Pawson T. Shc proteins are phosphorylated and regulated by the v-Src and v-Fps protein-tyrosine kinases. *Proc Natl Acad Sci USA* 1992; **89**: 8869–73.
31 Corson TW, Huang A, Tsao MS, Gallie BL. KIF14 is a candidate oncogene in the 1q minimal region of genomic gain in multiple cancers. *Oncogene* 2005; **24**: 4741–53.
32 Laurie NA, Donovan SL, Shih CS *et al*. Inactivation of the p53 pathway in retinoblastoma. *Nature* 2006; **444**: 61–6.
33 Scott D, Elsden J, Pearson A, Lunec J. Genes co-amplified with MYCN in neuroblastoma: silent passengers or co-determinants of phenotype? *Cancer Lett* 2003; **197**: 81–6.
34 Godbout R, Packer M, Bie W. Overexpression of a DEAD box protein (DDX1) in neuroblastoma and retinoblastoma cell lines. *J Biol Chem* 1998; **273**: 21 161–8.
35 Hsu T, Trojanowska M, Watson DK. Ets proteins in biological control and cancer. *J Cell Biochem* 2004; **91**: 896–903.
36 Oikawa T, Yamada T. Molecular biology of the Ets family of transcription factors. *Gene* 2003; **303**: 11–34.
37 Yendamuri S, Trapasso F, Calin GA. ARLTS1 – a novel tumor suppressor gene. *Cancer Lett* 2008; **264**: 11–20.
38 Calin GA, Trapasso F, Shimizu M *et al*. Familial cancer associated with a polymorphism in ARLTS1. *N Engl J Med* 2005; **352**: 1667–76.
39 Frank B, Meyer P, Boettger MB *et al*. ARLTS1 variants and melanoma risk. *Int J Cancer* 2006; **119**: 1736–7.
40 Petrocca F, Iliopoulos D, Qin HR *et al*. Alterations of the tumor suppressor gene ARLTS1 in ovarian cancer. *Cancer Res* 2006; **66**: 10 287–91.
41 Yendamuri S, Trapasso F, Ferracin M *et al*. Tumor suppressor functions of ARLTS1 in lung cancers. *Cancer Res* 2007; **67**: 7738–45.
42 Bellan C, De Falco G, Tosi GM *et al*. Missing expression of pRb2/p130 in human retinoblastomas is associated with reduced apoptosis and lesser differentiation. *Invest Ophthalmol Vis Sci* 2002; **43**: 3602–8.
43 Tosi GM, Trimarchi C, Macaluso M *et al*. Genetic and epigenetic alterations of RB2/p130 tumor suppressor gene in human sporadic retinoblastoma: implications for pathogenesis and therapeutic approach. *Oncogene* 2005; **24**: 5827–36.
44 MacPherson D, Sage J, Kim T, Ho D, McLaughlin ME, Jacks T. Cell type-specific effects of Rb deletion in the murine retina. *Genes Dev* 2004; **18**: 1681–94.
45 Brummelkamp TR, Nijman SM, Dirac AM, Bernards R. Loss of the cylindromatosis tumour suppressor inhibits apoptosis by activating NF-κB. *Nature* 2003; **424**: 797–801.
46 Weaver BA, Cleveland DW. Aneuploidy: instigator and inhibitor of tumorigenesis. *Cancer Res* 2007; **67**: 10 103–5.
47 Riggins GJ, Thiagalingam S, Rozenblum E *et al*. Mad-related genes in the human. *Nat Genet* 1996; **13**: 347–9.
48 Chan GK, Liu ST, Yen TJ. Kinetochore structure and function. *Trends Cell Biol* 2005; **15**: 589–98.
49 van Deursen JM. Rb loss causes cancer by driving mitosis mad. *Cancer Cell* 2007; **11**: 1–3.
50 Kapic A, Helmbold H, Reimer R, Klotzsche O, Deppert W, Bohn W. Cooperation between p53 and p130 (Rb2) in induction of cellular senescence. *Cell Death Differ* 2006; **13**: 324–34.
51 LaCasse EC, Baird S, Korneluk RG, MacKenzie AE. The inhibitors of apoptosis (IAPs) and their emerging role in cancer. *Oncogene* 1998; **17**: 3247–59.
52 Gstaiger M, Jordan R, Lim M *et al*. Skp2 is oncogenic and overexpressed in human cancers. *Proc Natl Acad Sci USA* 2001; **98**: 5043–8.
53 Sutterluty H, Chatelain E, Marti A *et al*. p45SKP2 promotes p27Kip1 degradation and induces S phase in quiescent cells. *Nat Cell Biol* 1999; **1**: 207–14.
54 Tsvetkov LM, Yeh KH, Lee SJ, Sun H, Zhang H. p27 (Kip1) ubiquitination and degradation is regulated by the SCF (Skp2) complex through phosphorylated Thr187 in p27. *Curr Biol* 1999; **9**: 661–4.
55 Carrano AC, Eytan E, Hershko A, Pagano M. SKP2 is required for ubiquitin-mediated degradation of the CDK inhibitor p27. *Nat Cell Biol* 1999; **1**: 193–9.
56 Alexander K, Hinds PW. Requirement for p27 (KIP1) in retinoblastoma protein-mediated senescence. *Mol Cell Biol* 2001; **21**: 3616–31.

Supporting Information

Additional Supporting Information may be found in the online version of this article:

Table 1. Primers and probe sequences for real-time quantitative polymerase chain reaction